Advance Publication Cover Page

Bulletin of the Chemical Society of Japan

Malachite Green Derivatives for Dye-sensitized Solar Cells: Optoelectronic Characterizations and Persistence on TiO_2

Jean-Baptiste Harlé,* Shuhei Arata, Shinya Mine, Takashi Kamegawa, Van Tay Nguyen, Takeshi Maeda, Hiroyuki Nakazumi, and Hideki Fujiwara*

Advance Publication on the web October 12, 2017
doi:10.1246/bcsj.20170289

Malachite Green Derivatives for Dye-sensitized Solar Cells: Optoelectronic Characterizations and Persistence on TiO_2

Jean-Baptiste Harlé,*[1] Shuhei Arata,[1] Shinya Mine,[2] Takashi Kamegawa,[2] Van Tay Nguyen,[3] Takeshi Maeda,[3] Hiroyuki Nakazumi,[3] and Hideki Fujiwara*[1]

[1]Department of Chemistry, Graduate School of Science, Osaka Prefecture University, 1-1 Gakuen-cho, Naka-ku, Sakai 599-8531

[2]Nanoscience and Nanotechnology Research Center, Osaka Prefecture University, 1-2 Gakuen-cho, Naka-ku, Sakai 599-8570

[3]Department of Applied Chemistry, Graduate School of Engineering, Osaka Prefecture University, 1-1 Gakuen-cho, Naka-ku, Sakai 599-8531

E-mail: jeanbaptiste.harle@gmail.com, hfuji@c.s.osakafu-u.ac.jp

Jean-Baptiste HARLE received his M. Sc. degree in 2013 from the university Pierre and Marie Curie (Paris VI). He then joined the Fujiwara Laboratory at Osaka Prefecture University, Japan to perform his Ph.D degree. His research interest encompasses the development of functional materials for dye-sensitized solar cells.

Hideki FUJIWARA received his Ph.D. (1999) from Kyoto University. He was appointed as a Research Associate at the Institute for Molecular Science in 1996 and moved to the Research Institute for Advanced Science and Technology, Osaka Prefecture University in 2003. Then he joined the Department of Chemistry, Osaka Prefecture University in 2005. He became a Lecturer (2006), an Associate Professor (2010) and a Professor (2016) of Osaka Prefecture University. He was awarded the Chemical Society of Japan Award for Young Chemists (2003).

Abstract

Derivatives of malachite green, a well-known triphenylmethine dye, have been adapted for third-generation photovoltaic applications as dye-sensitized solar cells (DSSC). The solar cells were developed based on a concentrated Br_3^-/Br^- liquid electrolyte coupled to different trifluoroacetate (TFA^-), triflate (TfO^-), bromide (Br^-) and tetrafluoroborate (BF_4^-) malachite green salts as dye sensitizers and mesoporous TiO_2 anatase as electron collector, and their optoelectronic properties were characterized. The adsorption patterns of such salts at the TiO_2 nanoparticles surface were studied by zeta (ζ) potential measurements on colloidal suspensions under neat conditions, and compared to the desorption rates of the dyes when exposed to the DSSC electrolyte. The different affinities of the ionic pairs for the oxide surface and the bulk were found crucial for the stability of the self-assembled monolayer of carboxylic acid-anchored chromophores at the surface, and for the photoconversion efficiency associated therewith. This study aimed at depicting the behaviour of the ionic pairs at the surface and gave insights for their physical and chemical stabilization in the DSSC environment.

1. Introduction

Malachite green (MG) and its analogs are hindered short-chain (monomethine) cyanine dyes, i.e. conjugated ionic type chromophores with an odd alternant system with two extreme resonance structures between two auxochromic nitrogens (Figure 1). It absorbs light at longer wavelength thanks to the strong bathochromic shift induced by the steric hindrance observed between the two N↔N-intrachain phenyl groups.[1] Although widespread,[2] mostly cost-effective and allowing light-harvesting in the visible light and at longer wavelength, triarylmethine dyes have been shown few interest for photovoltaic applications. Only a few examples like Eosin Y,[3] Rhodamine,[4-8] Phloxine B and Bromophenol Blue[9] or Rose Bengal[10] and Pyrogallol Red[11-13] dyes were reported available for sensitization in the standard nanocrystalline TiO_2 anatase-based DSSC. Malachite green and a few other derivatives have been considered for sensitization in a SnO_2-liquid junction-based cell[8] and recently inserted in CdS-based[7, 14] and Zr-doped $SrTiO_3$ photovoltaic technologies.[15] Sensitization using Ru-based complexes with free or surface-bounded counterions have been carried out by M. Grätzel and outlined the impact of their nature on the cells performances,[16, 17] but the studies neglected the impact of the counterions on the ionic distribution within the electrical double layer and their influence on the adsorption energetics of the dyes at the surface. Regulation of the diffuse ion swarm across the dye monolayer has a bearing on the motion of ions and the concentration gradients of the electrolyte and hence directly impacts the electron transfers at the TiO_2/dye/electrolyte interface.[18] Therefore, to investigate the role of the counterions under DSSC conditions, we synthesized new malachite green dyes **1**, **2** (Figures 1, 2) with a series of free (BF_4^-, Br^-) and adsorption-capable (TfO^-, TFA^-) counterions. The cationic structures of **1Me**$^+$, **1Dec**$^+$ and **2Me**$^+$ were derived from malachite green and adapted for n-type dye-sensitized solar cell (DSSC) sensitization with different 4-carboxyphenyl (**1**) and 5-carboxythiophen-2-yl (**2**) groups as acceptor/anchor moieties, and *n*-decyl hydrophobic moieties. The photoinactive counterions were found to play a significant role in the photoconversion capacity of the devices developed for this study as well as on the adsorption/desorption rates of the cationic chromophores.

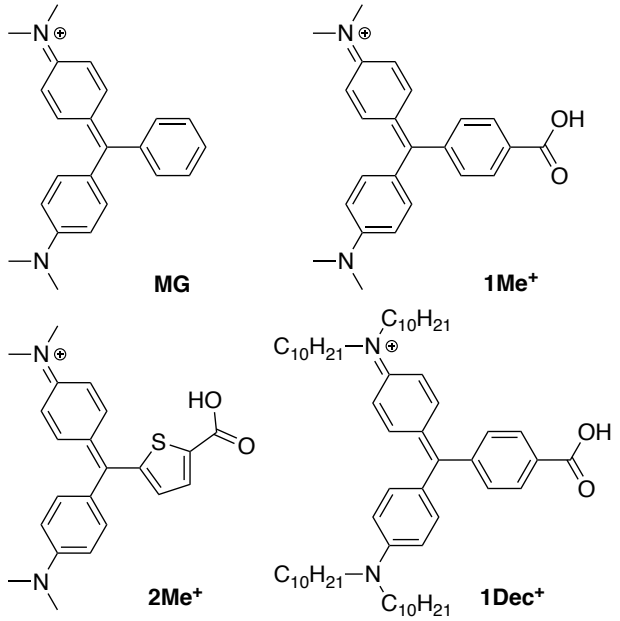

Figure 1. Chemical structures of malachite green **MG** and its derivatives **1Me**$^+$, **2Me**$^+$ and **1Dec**$^+$ developed for the present study and represented in their quinonoidal form.

2. Experimental

General procedures. All syntheses were performed under nitrogen atmosphere for safety reasons unless otherwise noted. Commercial reagents used for the syntheses were purchased from Tokyo Chemical Industries Ltd., Nacalai Tesque Inc. or Wako Pure Chemical Industries and used as received. 18NR-T transparent and PST-400C opaque titania pastes and FTO-coated TEC7 and TEC8 plates were purchased from Dyesol Ltd. ^{1}H NMR were recorded on JEOL JNM-400 400 MHz and VARIAN 400 MHz instruments with tetramethylsilane (TMS, δ = 0 ppm) as reference. ^{13}C NMR spectra were recorded on a JEOL JNM-400 MHz instrument with signal of solvents [$CDCl_3$ (δ = 77.16 ppm) or CD_3CN (δ = 116.79 ppm)][19] as reference. $CDCl_3$ was used as a deuterated NMR solvent of every synthetic intermediates and **1Dec-TfO**. All other malachite green's NMR samples were prepared with dry CD_3CN prepared as follows: 3Å molecular sieves[20] were heated *in vacuo* overnight to 200 °C, allowed to cool down to room temperature and poured in a nitrogen-filled Schlenk flask. A volume of commercial CD_3CN up to twice the volume of molecular sieves was poured inside under nitrogen flow, and the system was left as-is for at least 24 h before use. High resolution mass spectra (HRMS) were collected with a JEOL mass spectrometer station JMS-700 through FAB$^+$ and FAB$^-$ mode using 3-nitrobenzyl alcohol as matrix.

Optoelectronic characterizations. UV/vis/near-IR absorption spectra were recorded on a UV-3600 spectrophotometer (Shimadzu Corp.). Sample quartz cuvettes with 1 cm path length sealed under argon atmosphere were used absorption measurements of 10^{-5} M dye solutions in superdry acetonitrile. Direct measurements of the absorption spectra of sensitized TiO_2 screens were performed under air conditions, and the spectra were collected prior to and after treatment with an electrolyte constituted of 1.00 M LiBr(H_2O), 0.05 M Br_2 in superdry acetonitrile. The dyes were desorbed from the screen by dipping the photoanode into 0.06 mL of the electrolyte solution, quenching the desorption at every 15 s with dry acetonitrile and drying the cell under argon flow for UV/vis/near-IR measurement under air conditions.

Fabrication of the electrodes. Colourless 3.2 mm (TEC8, Dyesol Ltd.) and 2.2 mm (TEC7, Dyesol Ltd.) thick soda-lime glass coated with FTO were used as conductive substrate for the front (photoanode) and back (counter electrode) contacts, respectively. The glasses were successively cleaned with soap, rinsed with tap water and washed with acetone and methanol and underwent oxidation with a UV-O_3 system for 20 min. The TEC8 plates were subsequently immersed in a 40 mM aqueous $TiCl_4$ solution and the bath was heated to 70 °C for 30 min and washed with deionized water and methanol and dried under vacuum. A rheological paste of TiO_2 nanoparticles (18NR-T transparent, Dyesol Ltd.) was screenprinted with a 90T mesh and dried for 5 min at 125 °C. After cooling to room temperature the screen-printing procedure was repeated and the plates were heated to 125 °C for 5 min. A third layer of light-scattering nanoparticles (PST-400C active-opaque, Dyesol Ltd.) was screenprinted over as the last photoactive layer of the square 0.25 cm^2 electrode, and the whole was heated to 125 °C for 5 min and sintered at 475 °C for 45 min. The photoanodes were treated once more with a 40 mM aqueous $TiCl_4$ solution, heated to 70 °C for 30 min, rinsed with deionized water and washed with acetone, and calcinated at 500 °C for 15 min. Platina was coated at the back-contact as follows: A 10^{-2} M hexachloroplatinic acid (H_2PtCl_6) ethanolic solution was poured dropwise on the TEC7 plates and kept still as the solvent evaporated, and the electrodes were heated for 15 min at 400 °C.

Photoelectrochemistry. The Br_3^-/Br^- electrolyte used as redox shuttle for the solar cells was of the same composition as for the above-described optoelectronic characterizations of the dry TiO_2 photoanode. Sensitization, sealing of the solar cells and storage of the electrolyte and TiO_2 photoanodes were carried out under argon atmosphere in order to avoid exposure to air and moisture. The TiO_2 screens were sensitized over 6 h with 3×10^{-4} M dye solutions with superdry CH_2Cl_2 as solvent for **1Me-TfO**, **1Me-TFA**, **1Me-BF$_4$** and **2Me-TfO**, superdry CH_3CN for **1Me-Br** and dry CCl_4 for **1Dec-TfO** for maximization of the density of dyes at the surface and in absence of coadsorbents. Subsequently, the cells were washed with the respective sensitization solvent and dried under argon flow. The sensitized photoanodes and the back-contacts were sealed together with Surlyn film, and the electrolyte was injected in the cells through pre-drilled holes at the back-contact. At last, the devices were sealed with a thin glass and Surlyn film before exposure to air for characterization. The solar cells were irradiated with a CEP 2000 AM1.5 solar simulator (Bunkoukeiki Co, Ltd., Japan) for every photocurrent measurement (J-V curve under light and dark conditions, IPCE spectra and electrochemical impedance spectroscopy (EIS)). EIS measurements were performed with application of a cathodic bias voltage equal to the V_{OC} value under dark conditions and without application of a cathodic bias voltage under light (AM1.5 one sun) conditions, and collected with a HZ-5000 automatic polarization system (Hokuto Denko).

Zeta potential measurements. The dye@TiO_2 samples were prepared under argon atmosphere: into each 10^{-4} M dye solution (10 mL) was injected a 10^{-8} M colloidal suspension of TiO_2 nanoparticles (0.5 mL), and the samples were left as such after homogenization for at least 6 h for coverage equilibrium. The resulting colloidal solutions containing 1 part of TiO_2 nanoparticles for 10^4 parts of dye were kept in ultrasonic-cleansed sealed flasks until use. Zeta potential measurements were performed on an ELSZ-DN2 (Otsuka Electronics, Japan) analyzer with bare and sensitized TiO_2 anatase colloidal suspensions under neat conditions.

3. Results and Discussion

3.1 General synthetic route to malachite green derivatives.

The two-steps synthetic route followed broadly used ways to synthesize malachite green, without any sharp modifications (Figure 2). It provides a fast and inexpensive synthesis to small, steady and panchromatic dye sensitizers: the first condensation that was carried out with a catalytic amount of mild Lewis acid $ZnCl_2$,[21, 22] at reflux for 24 h in an ethanolic solution gave the Leuco compounds **Leuco-Me**, **LeucoT-Me** and **Leuco-Dec** in 65%, 52% and 39% yields, respectively. A solvent mixture of ethanol/*n*-butanol (1/1, v/v) was used for the condensation of the **Leuco-Dec** derivative for solubilization issues. The same reaction carried out in pure butanol afforded the condensate in 10% yield only, suggesting that the hydrophilic character of the solvent was of importance for the execution of the condensation. The following two-electron oxidation process[23] was merely carried out at room temperature with chloranil[22, 24] as a mild oxidant with one equivalent of the corresponding acids, namely triflic acid (TfOH), 42 wt% aqueous tetrafluoroboric acid (HBF_4), trifluoroacetic acid (TFA) or 48 wt% aqueous hydrobromic acid. Unlike the synthesis of methine dyes carried out by Kast et al.[24] in pure glacial acetic acid as solvent (hence in great excess), only one equivalent of each corresponding superacids was added to the medium in order to avoid undesired protonation of the tertiary amine function.[25] The oxidation yields correlated neither with slowlier kinetics due to the use of weaker acids and the size of the *N*-substituents nor with any difficulty to oxidize due to steric hindrance of the orthogonal substituents,[26, 27] and most likely relied to a large extent upon the different conditions for recrystallization. Pure black flickering compounds were obtained by slow elution with a solvent/non-solvent bilayer solution: CCl_4/hexane for **1Dec-TfO** and CH_2Cl_2/hexane for all **2Me**$^+$ and **1Me**$^+$ derivatives except **1Me-Br** that - due to solubility reasons - was recrystallized in a benzonitrile/benzene mixture. Oxidation trials with excess PbO_2 in the same conditions yielded the target compounds together with decomposition impurities, consistent with the observations made by Parvin, B. et al.[28] Tetrachlorohydroquinone (Cl_4HQ) could not be isolated from the synthetic mixture in the case of **1Me-Br** because of the poor solubility of the dye in low polarity solvents, and was observed in the crystalline lattice of

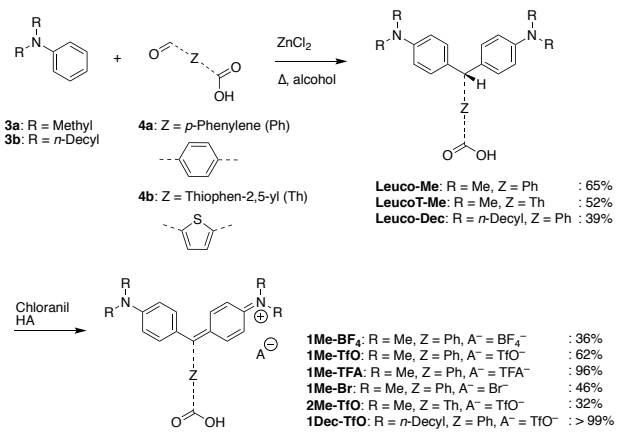

Figure 2. General synthetic route to malachite green derivatives **1** (Z = *p*-Phenylene) and **2** (Z = Thiophen-2,5-yl). The monomethine dyes were isolated as triflate (TfO^-), tetrafluoroborate (BF_4^-), trifluoroacetate (TFA^-) and bromine (Br^-) salts.

1Me-Br in 1:1 stoichiometry with the dye but did not appear in any other dye characterization. Stabilization of the oxidized form of the malachite green derivatives was observed under argon atmosphere in polar, superdry solvents like acetonitrile, benzonitrile or even methylene chloride. The low lightfastness products faded within a few hours in any solvent in the presence of oxygen, in accordance with literature.[2, 29] The phenomenon was accelerated in low polarity solvents like tetrahydrofuran or chloroform, consistent with a photolysis rate rising with the concentration and lifespan of the dioxygen excited singlet state[30] or other radicals[2] in low polarity solvents, phenomenon also increased by moisture.[2, 31]

3.2 Molecular structure and spectral properties of the dyes.

An X-ray crystal structure analysis was performed on a block-like single crystal of **1Me-Br** recrystallized from benzonitrile/benzene. The structure of this malachite green dye was slightly modified in order to adapt for sensitization in n-type Grätzel cells: A mere grafting of a carboxylic acid on the para position of the phenyl group that is orthogonal to the $N_1 \leftrightarrow N_2$ intrachain provided the dye a strong adsorption potential, red-shifted the S0→S1 (*x* band) absorption band[32-34] by 10 nm (λ_{max}(**MG**) = 619 nm,[35] λ_{max}(**1Me**$^+$) = 629 nm) as shown in **Table 1** and induced a small distortion in the triphenylmethine structure by comparison with the pure C_{2v} symmetry of the **MG** dye (Figure 4). In the solid state, differences between bond angles of the central sp^2 methine of

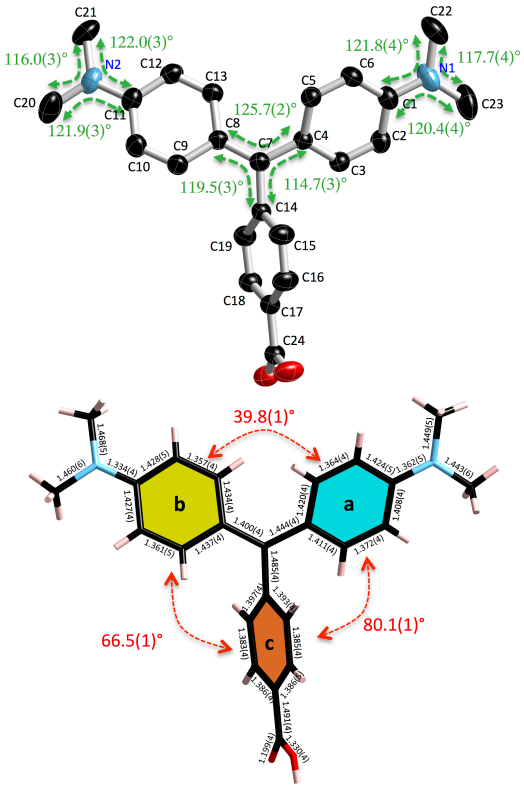

Figure 3. Single-crystal XRD-resolved coordinates of the molecular structure of **1Me**$^+$ (from **1Me-Br·Cl$_4$HQ salt**) Top: ORTEP drawing of the molecular structure with bond angles of the N1- and N2-centered sp^2 amine/aminium and C7-centered methine systems. Hydrogens were omitted for clarity. Black = carbon, Blue = nitrogen, Red = oxygen. Bottom: bond lengths and dihedral angles between the three *a*, *b* and *c* phenyl planes. The number in brackets for bond lengths and angles represents the error on the last digit.

1Me$^+$ (C8 - C7 - C4 = 125.7(2)°, C4 - C7 - C14 = 114.7(3)°, C14 - C7 - C8 = 119.5(3)°) and torsional angles between planes ($a \wedge b$ = 39.8(1)°, $b \wedge c$ = 66.5(1)°, $a \wedge c$ = 80.1(1)°) outlined the distortion of the triphenylmethine system induced by the intrinsic dissymmetry of the carboxylic acid (Figure 3) and the heterogeneous distribution of the counterions. The bromine atoms, although all equivalent in the $P2_1/c$ lattice of **1Me-Br·Cl$_4$HQ** (Figure S1, ESI) were unequally distant to the N1- and N2-centered aminium moieties of **1Me**$^+$: N2 - Br1 [4.593 Å, 5.103 Å, 4.878 Å] and N1 - Br1 [5.123 Å, 5.439 Å]. Hence, the cationic charge was greater on N2 as witnessed by the different bond lengths in the aniline moieties: the quinonoid character of phenyl *b* was more important than for phenyl *a* (C7 - C8 [1.400(4) Å] < C7 - C4 [1.444(4) Å], C9 - C10 [1.361(5) Å] < C3 - C2 [1.372(4) Å], C12 - C13 [1.357(4) Å] < C5 - C6 [1.364(4) Å], C11 - N2 [1.334(4) Å] < C1 - N1 [1.362(5) Å]) and at the same time participates at the destabilization of the cationic π -system. The global distortion induced by the electronic effect of the carboxylic acid was only small compared to the environment heterogeneity observed in the crystal, as observed by DFT studies: the distribution of the HOMO isodensity was homogeneously spread over the cyanine chain when optimizing the structure by DFT in adiabatic conditions (Figure 4). Furthermore, the dihedral angle between planes *a* and *b* of **1Me**$^+$ was observed much larger than in the crystal structure (+ 9.4°) whilst dihedral angles $a \wedge c$ and $b \wedge c$ were reduced by c.a. 18.1° and 4.6°, respectively. As seen in Figure 5, the substitution of the orthogonal phenyl ring by a thiophen-2,5-yl moiety red-shifted λ_{max} by 2 nm only (λ_{max} (**2Me**$^+$) = 631 nm). However the substitution of the four *N*-methyl groups by *N*-decyl substituents induced an 18 nm red-shift (λ_{max} (**1Dec**$^+$) = 647 nm), consistent with literature[36] and in accordance with the Dewar-Knott empirical rules for spectral changes relative to steric hindrance and electronic effects.[1, 37] The observed λ_{max} (*x* band) and *y* band red-shifts were mostly induced by the more electron-inductive character of the *N*-decyl substituents for **1Dec**$^+$ and the more electron-accepting thiophene moiety in **2Me**$^+$, respectively. The twisting of the *a* and *b* phenyl rings did not result in a more localized electronic charge on the auxochromic nitrogens, phenomenon observed by D. R. Waring & al[26] and likely had no bearing on the spectral parameters of these cyanine chromophores. As observed by density functional theory (Figure 4 and Table S3, ESI): the Mulliken charges on the auxochromes were calculated equivalent (δ(N) = –0.497) in **2Me**$^+$ and **1Me**$^+$ despite a +4.2° bathochromic torsional strain of the $a \wedge b$ angle in the **2Me**$^+$ derivative. The *N*-decyl substituents were responsible for the more important Mulliken charges (δ(N1) = –0.528, δ(N2) = –0.526) on the auxochromes in **1Dec**$^+$.

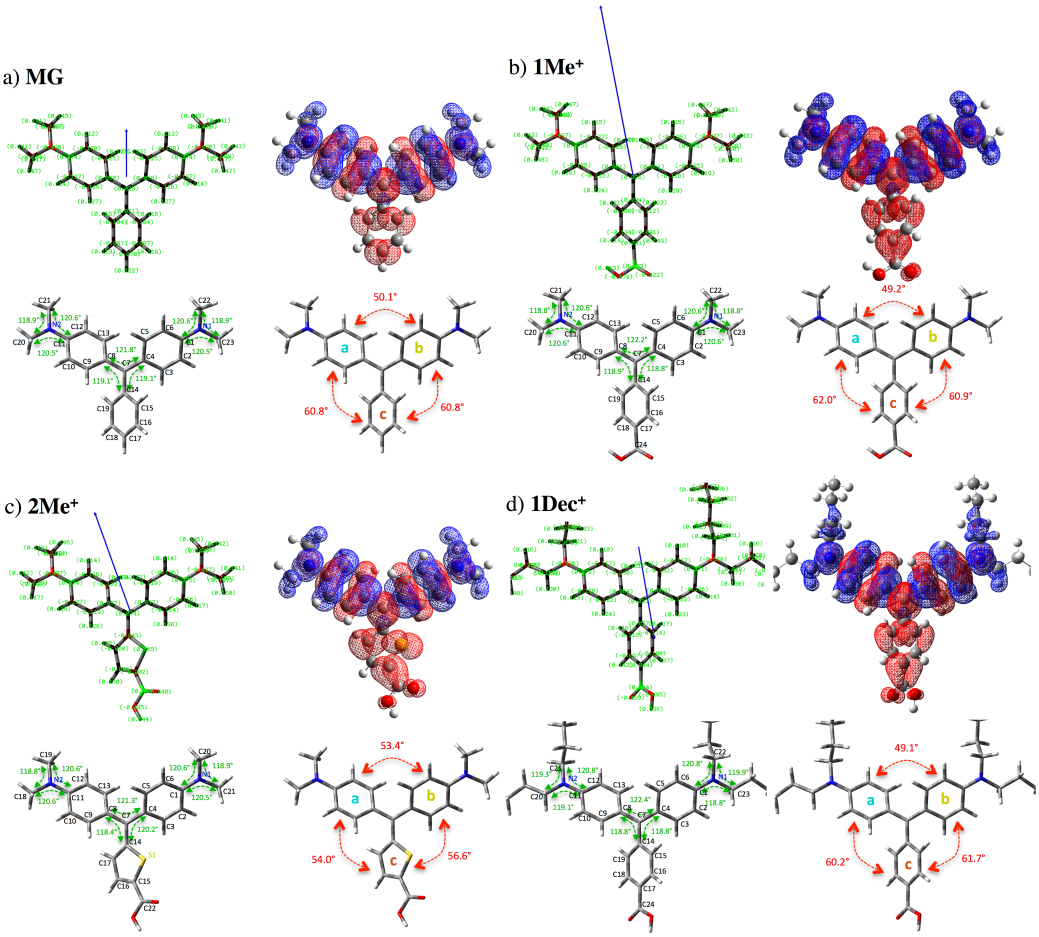

Figure 4. DFT-optimized molecular structures of the a) **MG**, b) **1Me**$^+$, c) **2Me**$^+$ and d) **1Dec**$^+$ cations. Top left: Mulliken atomic charge numbers; the atoms are coloured over a range of colours from red (–0.650) to green (+0.650). The origin of the permanent dipole moment vector is the center of the global electronic charge. Top right: front view of the HOMO (blue) and LUMO (red) isodensities, computed by DFT calculations with B3LYP 6-31G**[38] as exchange correlation functional and basis set; isodensity contour (solid) = 0.02. Absolute values of the bond angles (bottom left, green) and dihedral angles (bottom right, orange) at the planar aminium and central carbon atoms are displayed in degrees. The long alkyl chains of **1Dec**$^+$ were truncated in the present figure for clarity.

Table 1. Optoelectronic parameters of the chromophores in solution.

Dye	x band[i] [nm]	ε_{max} (x) [$M^{-1}cm^{-1}$]	y band[i] [nm]	ε_{max} (y) [$M^{-1}cm^{-1}$]	$E_{(S+/S)}$[j] [V vs NHE]	$E_{(0-0)}$[k] [V] (Abs/Em)	$E_{(S+/S*)}$[l] [V vs NHE]
1Me$^+$	629	50050	427	10940	1.41	1.88	-0.47
1Dec$^+$	647	46190	430	8220	1.43	1.84	-0.41
2Me$^+$	631	29500	482	11570	1.44	1.75	-0.31

[i] Wavelengths of peak maxima collected from absorption spectra of dyes in superdry acetonitrile solutions.
[j] The ground state redox potentials, measured with cyclic voltammetry (CV) under the following conditions: Pt counter electrode and Pt working electrode, Ag/AgCl reference electrode; electrolyte, 0.1 M recrystallized $TBAClO_4$ in benzonitrile (the benzonitrile was chromatographed on Alumina N Akt. I column before use. Potentials measured vs Ag/AgCl were corrected with ferrocene Fc/Fc^+ ($E_{(Fc/Fc+)}$ = 0.48V) and converted to NHE by addition of +0.241V. Cyclic voltammograms of the dyes are shown in Figure S2 (ESI).
[k] 0-0 transition energy ($E_{(0-0)}$) was issued from the energy value at 10% of the main peak intensity.
[l] LUMO energies ($E_{(S+/S*)}$) estimated vs NHE from the ground state oxidation potential added to $E_{(0-0)}$.

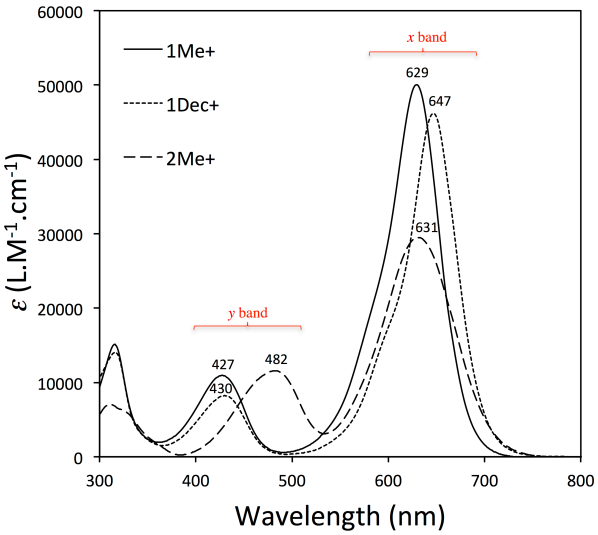

Figure 5. UV-Vis spectra of 10^{-5} M dye solutions in superdry CH_3CN. All measurements were performed under argon atmosphere with sealed 1 cm path length quartz cuvettes.

3.3 Lability of the chromophores in DSSC conditions

Unlike the black dye,[39] N719[40, 41] or most Ruthenium polypyridyl complexes[16, 42] developed for DSSC sensitization, the majority of developed organic dyes are designed with a lone carboxylic acid as an anchoring moiety for synthetic simplicity and efficiency.[43] Without any efficient chelation to contribute to the stabilization of the dyes at the electrolyte/dye/TiO_2 interface, the dye has a propensity to be driven away to the bulk. More specifically, the dye adsorbed at the surface is in equilibrium with the dye dissolved in the electrolyte. J. H. Park et al.[44] directly addressed this problem by merely adding some dye to the electrolyte prior to mounting the cell and showed a significant stabilization of every parameter of the cells. The thermodynamics of the dye adsorption/desorption process are significantly dependent - among many parameters - on heat, illumination, nature of the solvent and surface-active species[41, 45, 46] and therefore all characterizations of the dye@TiO_2 systems in this study were performed at room temperature, without any surface-active species in the electrolyte nor any coadsorbent other than the chromophore and its counterion. The chromophore's behaviour was thus function of the nature of its lone counterion and reciprocally, i.e. the adsorption and desorption rates of the chromophore and its counterion only depended on one another. Long-term cell degradation involving the device sealing, leakage and dye/electrolyte degradations were left outside of the scope of this study. Figure 6 highlights the evolution of the absorption patterns of the coloured TiO_2 screens as a function of the immersion time in the DSSC electrolyte (1.00 M $LiBr(H_2O)$ / 0.05 M Br_2 in superdry CH_3CN): The screens were dipped in the electrolyte to desorb the dyes for 15 s and rinsed in pure, superdry CH_3CN to quench the desorption to carry out the UV-Vis measurement (no desorption was observed in pure CH_3CN). This simple operation was repeated over a total 3 min time span to observe the desorption patterns of the dyes on a short time scale. For given chromophores, the desorption rates sharply differed from one counterion to another: for instance, the **1Me-BF$_4$**-sensitized TiO_2 screen was utterly bleached after the 3 min time span, suggesting that nearly all the chromophores were desorbed whereas the **1Me-TFA**-sensitized screen remained dark green. Although the chromophore's structure (**1Me$^+$**) remains unchanged and hence its physico-chemical properties were identical, the desorption rates were observed quite different. This observation underlined the fact that the use of a lone carboxylic acid as the anchor leaves these chromophores highly dependent to small changes in their environment.

In a mesoporous semi-infinite domain, namely, nanocrystalline TiO_2 considered as an impermeable solid and the electrolyte as the bulk in the present case, the space distribution of ions proximate to the interface is function of cohesive and dispersive forces. Unfortunately, under such high ionic strength (> 1 M) of the DSSC condition the Debye-Hückel point-charge approximation[47] doesn't hold and the ionic interactions ought to be considered and thus neither the Gouy-Chapman,[48, 49] the Grahame Langmuir,[50] the hypernetted-chain theory based on the Ornstein-Zernike equations[51] nor any other theory can accurately describe the system from a purely theoretical point of view, to the best of our knowledge.[52-55] Ionic adsorbates binding to the surface of a particle form a quasi-monolayer governed by their relative size and charge:[56] the bounding process can be described by a Langmuir-type adsorption isotherm relating fractional surface coverage Θ_f to the adsorbate concentration C with respect to the equation:

$$\Theta_f = \frac{\kappa C}{1 + \kappa C}$$

with κ as the ratio of adsorption/desorption for a given ionic

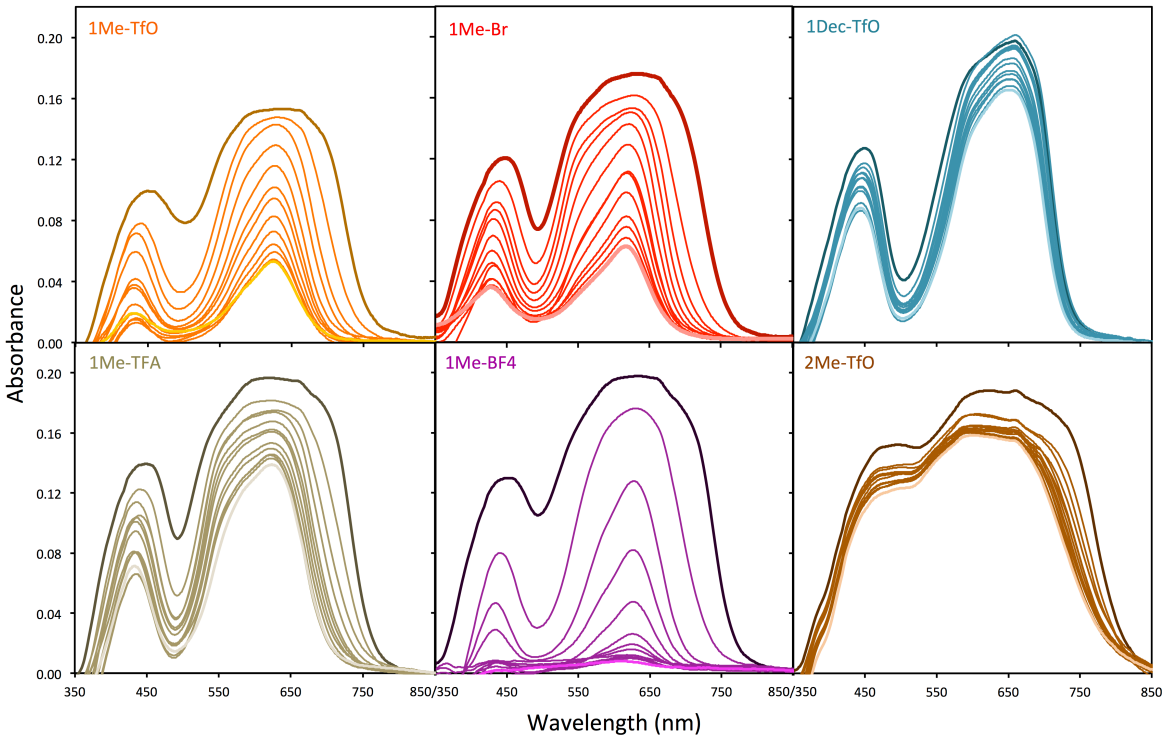

Figure 6. Plotting of the desorption of the dyes from the TiO_2 nanoparticles screen over time when dipped into 0.06 mL of an electrolyte constituted of 1.00 M $LiBr(H_2O)$ / 0.05 M Br_2 in superdry CH_3CN, followed by UV-Visible absorption spectra measurement. The absorption spectra were recorded every 15 seconds over a 3 min time span, as the desorption was quenched by rinsing the cells in superdry CH_3CN.

species. Only in the case of an ionic pair A the adsorption of one of the two ions encompasses the properties of both, and κ can be expressed as:

$$\kappa = \frac{[AS]}{[A][S]}$$

with $[AS]$ and $[S]$ corresponding to the surface densities of all occupied and unoccupied sites at the surface of the particle, respectively. In the case where both the cation and the anion possess an adsorption potential, the adsorption processes cannot be merely described inasmuch as (i) the fractional surface coverages may depend on one another, (ii) the versatile adsorbates may occupy different adsorption sites and (iii) the interaction between adsorbates may not be neglected. However, in the globally electroneutral system the concentration of one ion at the surface raises an electric potential Φ_0 and implies the building of an opposed nearby potential Φ_{diff} (Figure 7). The zeta (ζ) potential of sensitized nanoparticles in colloidal suspensions, related by nature to those potentials, was experimentally available to qualitatively determine the excess species in the diffuse layer and thus at the surface. As previously seen for other streptocyanine derivatives,[57] the zeta potential shift ($\Delta\zeta$) relative to bare TiO_2 nanoparticles (ζ_{TiO2} = 4.33 ± 2.05 mV) is directly correlated to the linkage patterns of the dye and of the same sign (positive or negative) as the excess species in the diffuse layer. Owing to electroneutrality, the global concentrations of the cations and the anions are equal and thus, the majority species in the diffuse layer is minority adjacent to the surface and reciprocally. In one case, both moieties of the ionic pair are potentially bounded to the surface (Figure 7a), and in the other case only the cation possess an adsorption potential and the free anion remains attracted to its counterion via Coulombic (electrostatic) interaction (Figure 7b): At the equilibrium, attractive forces (adsorption, electrostatic, van der Waals and so on) are balanced out by the diffusive forces such as osmosis, solvation, electrostatic repulsion. Sensitization with the TfO- and TFA-based species (**1Me-TfO** and **1Me-TFA**) shifted the zeta potential towards more positive values whereas the BF_4- and Br-based species (**1Me-BF$_4$** and **1Me-Br**) shifted the zeta potential of the nanoparticles downward (Figure 8, left and Table 2), indicating that the excess species in the diffuse layer were the chromophores **1Me$^+$** and **2Me$^+$** in the case of TfO- and TFA-based species and the photoinactive moieties BF_4^- and Br^- for the compounds **1Me-BF$_4$** and **1Me-Br**, respectively. BF_4^- is generally considered as a non-complexing anion[58] and likely to be indifferent to the TiO_2 anatase surface in the present study. The Br^- anion may display weak interactions with the surface in such anhydrous and concentrated conditions,[59] however these can be neglected compared to the adsorption potential of **1Me$^+$**. Therefore, the adsorption/desorption kinetics of their respective **1Me-BF$_4$** and **1Me-Br** salts mostly relied upon the adsorption strength of **1Me$^+$** and the affinity to the bulk of both the anion and the cation. After 1 min dip in the Br_3^-/Br^- electrolyte, the absorption intensity of the monomer peak of **1Me-BF$_4$** (624 nm) decreased by 76% against a 23% drop for **1Me-Br** (Figure 8, right). Zeta potential measurements of **1Dec-TfO**-sensitized nanoparticles suspended in superdry acetonitrile were unsuccessful: the electro-optic sampling (EOS) signal was nearly flat, probably accounting for the insolubility of such lipophilic dye@TiO_2 system, but this property was also likely responsible for the best stability observed for such system. The intensity of the monomer peak of **1Dec$^+$** (654 nm) only decreased by 3.5% after 1 min dip in the electrolyte and by 15% after 3 min dip against a 65% drop for the methyl derivative **1Me-TfO**. Interestingly, the **1Me$^+$** chromophore was best stabilized with TFA^- as counterion: the derivative **1Me-TFA** only displayed a 29% drop in intensity (Figure 8).

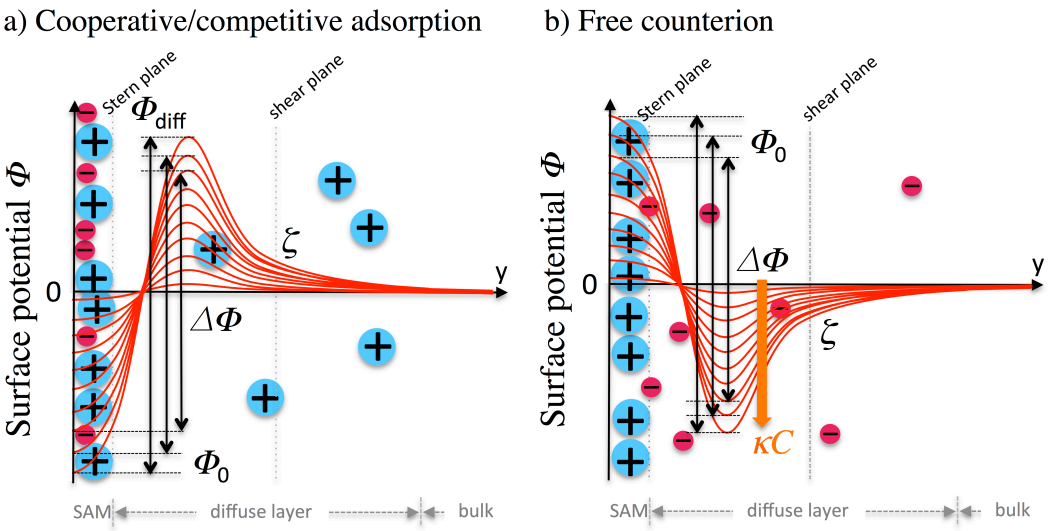

Figure 7. Representation of the surface potential Φ patterns with respect to the distance to the surface y and function of the ionic distributions a) at the surface for TiO_2 coadsorbed by cations and anions and b) at the surface where cations adsorbed at the TiO_2 surface and free anions with $\Delta\Phi$ as the difference between the surface potential Φ_0 and the diffuse layer potential Φ_{diff}. Only the excess species are represented in the diffuse layer and the bulk.

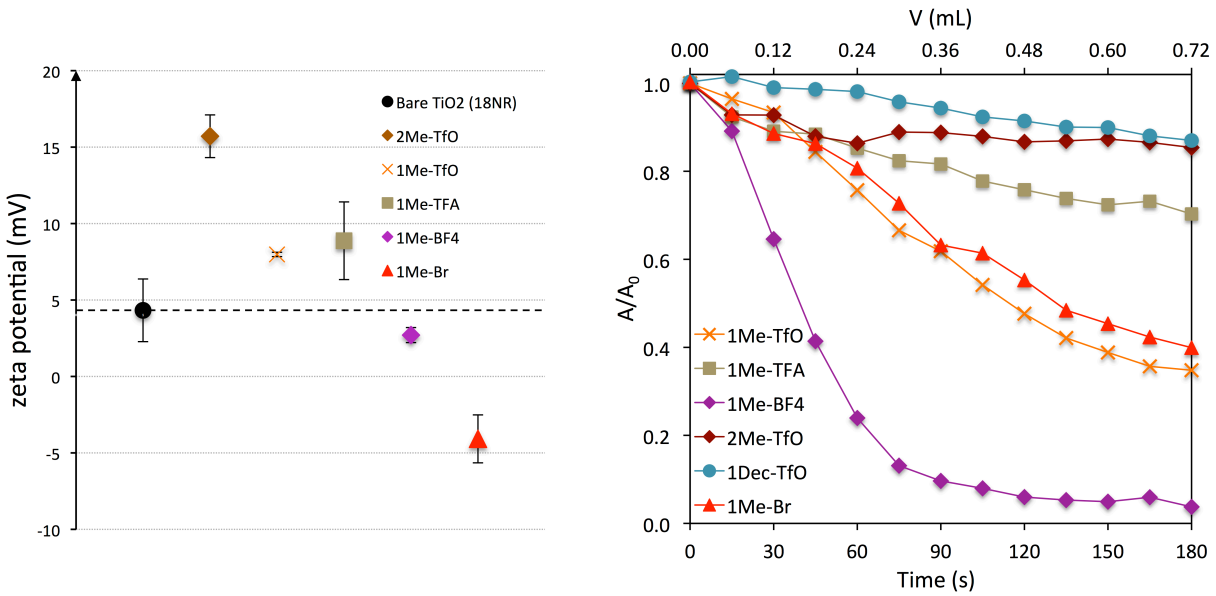

Figure 8. *Left*. Averaged values of at least two zeta potential measurements of colloidal suspensions of bare - and sensitized with **2Me-TfO**, **1Me-TfO**, **1Me-TFA**, **1Me-BF$_4$** and **1Me-Br** - TiO_2 anatase nanoparticles in superdry acetonitrile. *Right*. Plotting of the desorption of the dyes from the TiO_2 screen when dipped in an electrolyte constituted of 1.00 M $LiBr(H_2O)$ and 0.05 M Br_2, followed by UV-Vis absorption measurements after quenching the desorption every 15 s by washing with dry acetonitrile (See also Figure 6). The absorption values at λ_{max} of the dyes@TiO_2, namely 596 nm for **2Me-TfO**, 624 nm for **1Me$^+$**-based dyes and 654 nm for **1Dec-TfO**, were normalized with respect to the initial value before dipping.

The affinity for the bulk/affinity for the surface ratio decreases in the order $BF_4^- > TfO^- > Br^- > TFA^-$ in these **1Me$^+$** salts and the minimum ratio was obtained with a carboxylic acid-anchored anion (TFA^-). The most stable adsorption mode of TFA^- calculated by De Angelis et al.[60] was a bridged bidentate mode whereas the sulfonate of TfO^- was likely adsorbed at the surface via a weaker bridged bidentate mode assisted by hydrogen bonding,[61] also consistent with the lower desorption rates of TFA- and TfO-based dyes. Although stabilized thanks to a work on the nature and properties of its counterions, the **1Me$^+$** chromophore could not be fully stabilized at the TiO_2 surface and better results could be obtained with *n*-decyl substituents as previously discussed with **1Dec$^+$** or with the thienyl derivative **2Me$^+$**. The three chromophores **1Me$^+$**, **1Dec$^+$** and **2Me$^+$** were linked to the TiO_2 surface with a lone carboxylic acid, usually adsorbed onto the surface in a dissociative bridging bidentate mode, with one proton transferred to a nearby surface oxygen.[60, 62] However, FT-IR studies did not help witnessing the adsorption mode of the dyes as the empirical Deacon and Philips attribution of any $\nu_{as}COO$ or ν_sCOO frequencies,[63] that was hindered by the overcharged spectra (Figure S3, ESI), and all peaks from 1800 to 3600 cm^{-1} in the dye@TiO_2 spectra were flattened out after adsorption on TiO_2 with the exception of the νC-H in the range 2800 - 3000 cm^{-1}.[16] In the case where the counterion is a triflate, the difference between desorption rates of all three

chromophores (**1Me-TfO**, **1Dec-TfO** and **2Me-TfO**) mostly relied upon their interactions with adsorbed co-ions and their affinity to the bulk. More specifically, the chromophores were stabilized at the surface either isolated (monomers) or as H- and J-aggregates, as witnessed by the UV-Vis absorption patterns of the dyes adsorbed on TiO_2. Except for **1Dec-TfO** for which only H-aggregation was observed with a shoulder around 580 nm, all dyes exhibited a monomer peak around 640 ~650 nm with two shoulders arising from H- and J-aggregation, at shorter and longer wavelength, respectively. During the desorption measurements, the intensity of the shoulder around 700 ~750 nm arising from the J-aggregation of the dyes decreased quicker than both the monomer peak and the shoulder of H-aggregated dyes around 550 nm. This drop was pre-eminent for the **1Me-TFA**, **1Me-Br** and **2Me-TfO** derivatives and lesser for **1Me-TfO** and **1Me-BF$_4$**. These observations suggested that the aggregation modes of the dyes may have a bearing on their stabilization at the surface and that J-aggregated ones had a greater propensity to desorption.

Table 2. Influence of the counterion natures on the ζ potential.

Dye@TiO_2	ζ_i (mV)	$\Delta\zeta_i$ ($\zeta_i - \zeta_{TiO2}$, mV)
2Me-TfO	+15.71 ± 1.40	+11.38 ± 3.45
1Me-TfO	+7.98 ± 0.14	+3.65 ± 2.19
1Me-TFA	+8.88 ± 2.54	+4.55 ± 4.59
1Me-BF$_4$	+2.71 ± 0.49	–1.62 ± 2.54
1Me-Br	–4.08 ± 1.57	–8.41 ± 3.62

The zeta (ζ) potential values are the average of at least two consecutive measurements in the same conditions with the corresponding standard deviation, and the combined standard deviation for the differential values ζ_i - ζ_{TiO2} (ζ_{TiO2} = 4.33 ± 2.05 mV).

3.4 Photovoltaic performances of DSSCs.

The photocurrent action spectra of the dye-coated nanocrystalline TiO_2 stacked electrodes are displayed in Figure 9, right together with the photocurrent (J) - voltage (V) characteristics curves of the cells (Figure 9, left) dipped in a Br_3^-/Br^--based electrolyte. Owing to its higher lying redox couple's energy level ($E(Br_3^-/Br^-)$ = +1.09 V vs NHE), the open-circuit voltage (V_{OC}) of the cells greatly improved from a best 0.20 V to 0.50 V when using this redox shuttle instead of the commonly used I_3^-/I^- couple. The wider energetic gap, allowing V_{OC} values as high as 1.21 V for a DSSC with this Br_3^-/Br^--based electrolyte as shown by Hanaya, M. et al,[64] between the electrolyte and the TiO_2 conduction band largely compensated for the small loss in short-circuit current density (J_{SC}). Sugihara et al.[3] first demonstrated in 2005 that a Br_3^-/Br^- redox shuttle should be preferred to I_3^-/I^- for sensitizers having a ground state oxidation potential more positive than that of Br_3^-/Br^-, which was the case of the three **1Me$^+$**, **1Dec$^+$** and **2Me$^+$** sensitizers: driving forces for electron recombination ΔE were calculated to be 0.32, 0.34 and 0.35 V, respectively with respect to the equation $\Delta E = E_{(S+/S)} - E_{(Br3/Br)}$, where the ground state redox potentials of the dyes $E_{(S+/S)}$ were 1.41, 1.43 and 1.44 V, respectively, as displayed in Table 1. Moreover, the photovoltaic activity of the cells were best improved at higher concentrations of the electrolyte (1.00 M LiBr(H_2O) / 0.05 M Br_2) than the electrolyte used by Sugihara et al., constituted of 0.4 M LiBr and 0.04 M Br_2 for their study with the well-known Eosin Y dye.[3] Higher concentrations of electrolyte did not lead to any improvement of the cell parameters due to limitations in recombination kinetics between the electrolyte and the oxidized dye. Further trials for improvement of the V_{OC} value with a well-known $Co^{II/III}$tris(bipyridyl)[65] electrolyte constituted of 0.25 M $[Co^{II}(tbp)_3](PF_6)_2$ / 0.025 M $[Co^{III}(tbp)_3](PF_6)_3$ in superdry acetonitrile did not lead to any significant photocurrent. The TiO_2 screens were sensitized in 0.3 mM dye solutions without any coadsorbent: for instance, the photoconversion was nearly quenched with addition of chenodeoxycholic acid (CDCA) in the dyeing bath. Furthermore, the addition of any coadsorbent might have impaired the study of the influence of the different TfO^-, TFA^-, BF_4^- and Br^- counterions on the cell's parameters.

As witnessed by comparison of the UV/vis/near-IR absorption spectra of the dye@TiO_2 screens (Figure 6) and the photocurrent action spectra (Figure 9, right), J-aggregates, although allowing light harvesting at longer wavelength, barely induced any photocurrent. J-aggregated cyanine dyes are

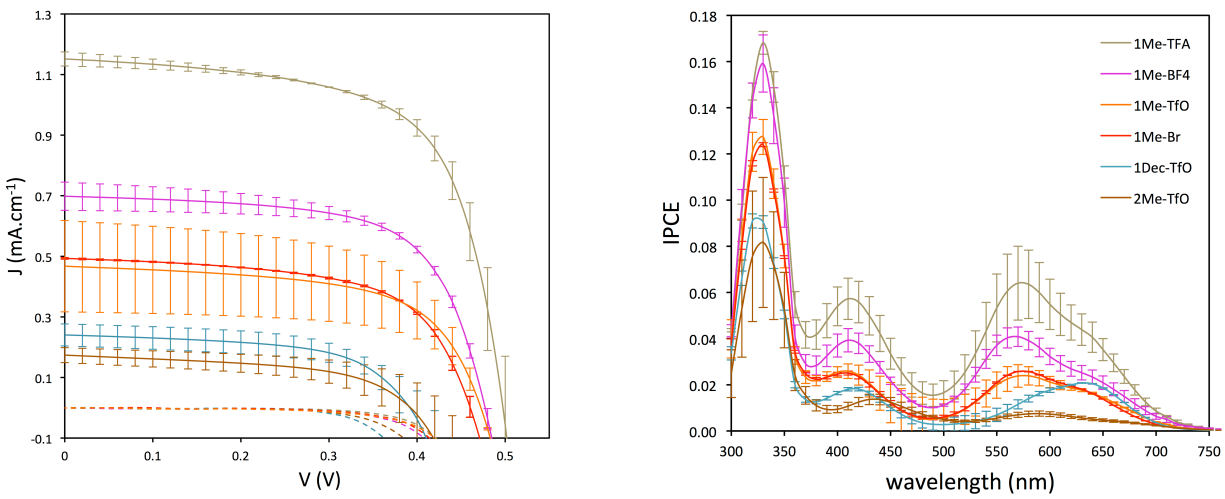

Figure 9. *left*: Photocurrent (J) -voltage (V) characteristics curves under AM 1.5 artificial sunlight source (plain) and dark conditions (dotted line) and *right*: IPCE action spectra for nanocrystalline TiO_2 solar cells sensitized under argon with the dye sensitizers dipped in 1.00 M LiBr(H_2O) / 0.05 M Br_2 in superdry CH_3CN. The error bars represent the standard deviation on the measurements obtained with at least two cells prepared under the very same condition. No further additives were used in the electrolyte.

usually photoactive in DSSCs, as formerly demonstrated with the efficient asymmetrical closed-chain cyanines,[66, 67] asymmetrical streptocyanines,[57] and hemicyanines,[68, 69] outlining their utility for sensitization of n-type Grätzel cells. In the present case their inactivity is presumably due to the aggregation-induced lack of driving force for electron migration from the lower-lying redox level of the J-aggregates excited state to the conduction band of TiO_2. The excited state level of the monomer $E_{(S+/S*)}$ was determined to be −0.47, −0.41 and −0.31 V vs NHE, respectively, for the chromophores **1Me**$^+$, **1Dec**$^+$ and **2Me**$^+$ by adding the zeroth-zeroth transition energy $E_{(0\text{-}0)}$ to the ground state oxidation potential $E_{(S+/S)}$ (Table 1). Owing to the ultrafast nonradiative relaxation dynamics of malachite green derivatives impeding fluorescence spectroscopy in the standard conditions as largely reported in the scientific literature,[2, 32-34, 70-72] $E_{(0\text{-}0)}$ was estimated from the energy value equivalent to the wavelength at 10% of the S0→S1 (*x*) band of the monomers in solution. Those values of $E_{(S+/S*)}$, too close to the Fermi level of TiO_2 at −0.50 V vs NHE[73] did not allow a saturation of the IPCE signal despite the high lithium concentration (1.00 M) in the medium[74] and thereby highlighted the different contributions of every electronic transition of monomeric and aggregated species to give rise to a photocurrent in the experiment conditions. Still, part of the low IPCE also accounted for the low light harvesting efficiency (LHE) of the devices (Figure S5, ESI) in spite of the good extinction coefficient of the dyes (Figure 5): Most optical densities of the dye monolayer@TiO_2 plateaued at 35%, except **1Me-Br** and **1Me-TfO** which displayed lower - 33% and 29%, respectively - LHEs at the maximum absorption wavelength. The best IPCE observed for every dye was observed around 330 nm, with a maximum value of 17% for the **1Me-TFA** derivative. At longer wavelength, the best photocurrents were attributed to the blue-shifted vibronic shoulder with absorption maxima ranging from 565 nm (**1Me-BF$_4$**) to 590 (**1Dec-TfO**) nm of the H-aggregated **1Me**$^+$ and **2Me**$^+$ chromophores, on average 1.5 times higher than the IPCE arising from the monomeric *x* band around 635 nm. The better photocurrents observed were attributive to the higher oxidation potential of the dyes in the H-aggregated regions of the self-assembled monolayer (SAM).[4-6, 12] Interestingly, the coadsorption of the chromophore and its counterion did not impede nor favoured the H- or J-aggregation. The photocurrents arising from the S0→S2 (*y* band) in the 410 - 440 nm region were as high as the photocurrents induced from the H-aggregates (Figure 9, right), and significantly blueshifted compared to the *y* bands in solution, 482, 430 and 427 nm for **2Me**$^+$, **1Dec**$^+$ and **1Me**$^+$ (Figure 5), respectively, although a red-shift was observed at high surface coverage on TiO_2 for this very band around 450 nm for **1Dec**$^+$ and **1Me**$^+$ and plateaued from 440 to 520 nm for **2Me**$^+$ (Figure 6). This discrepancy can be explained from the fact that the UV/vis/near-IR measurements were performed under dry conditions and that the *y* band, with a strong charge-transfer character is highly sensitive to its environment and largely blue-shifted under DSSC conditions, namely, when the solar cell is dipped into the highly ionic electrolyte. The accepting/anchoring moiety - orthogonal to the N↔N intrachain - of every dye bears the largest isodensity coefficient of the LUMO+1 (S2) state and allows facile injection into the semiconductor's conduction band. The efficiency (η) of the DSSCs sensitized with **1Me**$^+$ salts ranged from 0.37(1)% for **1Me-TFA** to 0.13(4)% for **1Me-TfO**, pointing out the role of the counterion not only on the cell stability as previously discussed but also on the cell's efficiency (Table 3). The better efficiency obtained with carboxylate-anchored (TFA^-) and sulfonate-anchored (TfO^-) counterions were consistent with the results of Huang and coworkers[69] with benzothiazolium hemicyanine dyes, albeit these dyes' counterions were covalently bound to the chromophore thanks to a short aliphatic chain. Devices sensitized with the **1Dec**$^+$ and **2Me**$^+$ chromophores showed lower photovoltaic conversion efficiencies (PCE) due to the thermodynamically unfavourable electron transfer from the dyes' excited states to TiO_2, correlating with the down shift of the dark currents and lower open circuit voltage (V_{OC}) values despite longer electron recombination lifetimes for both derivatives, respectively 0.465 and 0.527 ms (Fig. S7 and Table 3) that were estimated using the Bode phase plot mentioned below. The best electron lifetime at the TiO_2/dye/electrolyte interface with **1Me**$^+$ derivatives was observed for **1Me-TfO** and **1Me-Br** with 0.379 ms. Fill factors as high as 0.65 could be achieved with both **1Me-TFA** or **1Me-BF$_4$** and barely dropped to 0.61 for both **1Me-TfO** and **1Me-Br**, demonstrating a good charge separation and screening at the TiO_2/dye/electrolyte interface and induced better series and shunt resistances for a malachite green-based device compared to the reported SnO_2-liquid junction[8] or porous CdS[7] technologies of DSSC.

Table 3. Photochemical properties of the cells under simulated AM 1.5 irradiation.

Dye	V_{OC} (V)	J_{SC} (mA cm^{-2})	V_{MAX} (V)	J_{MAX} (mA cm^{-2})	*ff*	τ (ms)	η (%)
1Me-TFA	0.50 ± 0.01	1.15 ± 0.03	0.39 ± 0.02	0.95 ± 0.01	0.65 ± 0.02	0.290	0.37 ± 0.01
1Me-BF$_4$	0.48 ± 0.01	0.70 ± 0.05	0.38 ± 0.00	0.57 ± 0.01	0.65 ± 0.04	0.366	0.22 ± 0.01
1Me-TfO	0.47 ± 0.00	0.48 ± 0.15	0.36 ± 0.00	0.37 ± 0.11	0.61 ± 0.02	0.379	0.13 ± 0.04
1Me-Br	0.46 ± 0.00	0.49 ± 0.00	0.37 ± 0.02	0.38 ± 0.00	0.61 ± 0.01	0.379	0.14 ± 0.00
1Dec-TfO	0.40 ± 0.02	0.24 ± 0.04	0.29 ± 0.01	0.21 ± 0.07	0.58 ± 0.03	0.465	0.06 ± 0.01
2Me-TfO	0.40 ± 0.04	0.17 ± 0.02	0.29 ± 0.04	0.12 ± 0.02	0.53 ± 0.04	0.527	0.04 ± 0.01

V_{OC}: open circuit voltage; J_{SC}: short circuit current density; $ff = (V_{MAX} \times J_{MAX})/(V_{OC} \times J_{SC})$: fill factor; τ: electron recombination lifetime; η: photoconversion efficiency. The error numbers correspond to the standard deviation of the measurements of at least two solar cells performed under the exact same conditions. All cells were fabricated under argon atmosphere were performed with a Br_3^-/Br^- electrolyte constituted of 1.00 M LiBr(H_2O) and 0.05 M Br_2 in superdry acetonitrile as electrolyte.

Electrochemical impedance spectroscopy was carried out under AM 1.5 one sun and dark conditions to visualize the charge-transfer/recombination processes in the devices, and shown in Figure 10 as Nyquist plots and in Figure S7 as Bode phase plots. In a device working with a Br_3^-/Br^- redox shuttle, the large semicircle corresponds to the charge-transfer resistances at the TiO_2/dye/electrolyte interface and generally bigger than with an I_3^-/I^- electrolyte.[3] The charge-transfer resistances at the interface under both AM 1.5 one sun and dark conditions increased, for the **1Me**$^+$ derivatives in the order **1Me-TFA** < **1Me-Br** < **1Me- TfO** < **1Me-BF$_4$**, outlining the strong effect of the counterion on the electron transfers. **1Me-TFA** showed the lowest charge transfer resistance, consistent with the increase in Jsc[75] and contributed at demonstrating that TFA^- was best suited for this chromophore. We also estimated the electron recombination lifetimes τ at the TiO_2/dye/electrolyte interface from the low angular frequency peaks in the Bode phase plot according to the Kern equation,[76] that leads $\tau = 1/(2\pi f)$, where f is the frequency peak of the superimposed ac voltage (Fig. S7, ESI and Table 3). The lifetimes of **1Me**$^+$ salts are estimated to be 0.366, 0.379, 0.379 and 0.290 ms for the BF_4^-, Br^-, TfO^- and TFA^- derivatives under AM 1.5 one sun illumination, respectively. They are correlated to recombinations kinetics of the injected electrons and in stark contrast with the cells parameters: The TfO^- and Br^- salts showed the same, longest electron lifetimes (ca. 0.379 ms) and gave similar Voc, Jsc, desorption rates and photoconversion efficiencies whereas the BF_4^- salt yielded a slightly lower electron lifetime (0.366 ms) altogether with an increase in Voc. Likewise, **1Me-TFA** showed the best stabilization on TiO_2 and the best Voc, inconsistent with its short electron lifetime. Evidently, in this case the lone electron lifetimes did not reflect the cell behaviors with such different current densities: an increase in Jsc induces a concomitant diminution of the electron lifetime and inversely.[77] The observed V_{OC} values did not follow the same trend and most likely arose from a limitation in recombination kinetics between the dye and the electrolyte as formerly observed by Detty, M. et al with chalcogenorhodamine dyes/iodine-iodide as sensitizer/electrolyte couples,[4, 5] howbeit monotonically increased together with J_{SC} and hence with the electronic population in the conduction band of TiO_2. The influence of the counterion on the charge transfer resistance was, in the present case more important than the induced loss in injected electron lifetimes. The origin of the difference in charge transfer/recombination ratio at the electrolyte/**1Me**$^+$/TiO_2 interface in function of the nature of the counterion could hardly be discussed at the present state of studies because several factors like partial dye desorption and difference in ionic distribution of the diffuse ion swarm proximate to the surface could not be set apart. Indeed, the impact of the electroactivity of the counterions on both the electric double layer, the surface quantum states and passivation of the surface were correlated to each other, and those quantities had to be considered together for discussion. Further experiments are required to distinguish and clear out the implications of each one of these parameters and explain the ordering of the photoconversion efficiencies: **1Me-TfO** < **1Me-Br** < **1Me-BF$_4$** < **1Me-TFA**. Anyway, the IPCE spectra showed a global raise/drop of the photoaction over the whole visible range while switching counterions, most likely ruling out their impact on the propensity to aggregate and the type of aggregation of the chromophores and impacting the general thermodynamics of electron transfers.

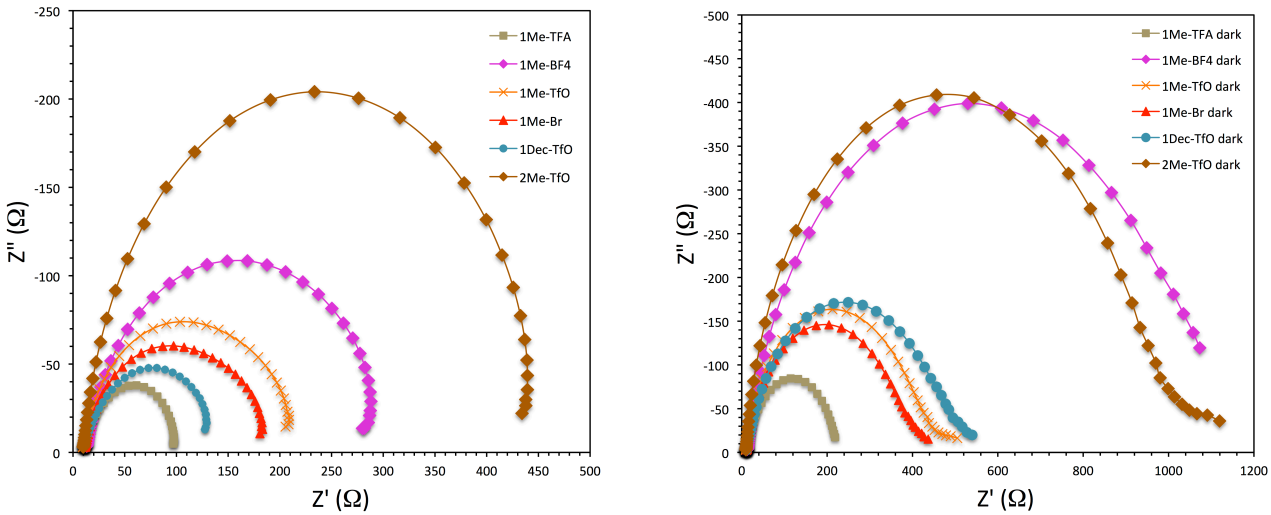

Figure 10. Nyquist plots of the solar cells measured under AM 1.5 one sun (*left*) and under dark (*right*) conditions.

4. Conclusion

Colouring of TiO_2-based n-type DSSC cells was performed for the first time with malachite green derivatives thanks to a mere grafting of carboxylic acid on the electron accepting/anchoring moiety of the chromophores. The **1Me**$^+$, **1Dec**$^+$ and **2Me**$^+$ chromophores were synthesized in a cost-effective two-steps synthetic route and isolated as TFA^-, TfO^-, BF_4^- and Br^- salts. DFT methods showed that the electronic isodensity of the different ground and excited states of the dyes looked alike from one chromophore to another and explained, to a large degree their similar optoelectronic properties. Investigation of the structure of **1Me**$^+$ by X-ray diffraction on a single crystal of **1Me-Br·Cl$_4$HQ** revealed, to the best of my knowledge the first crystal structure determined for a malachite green derivative. Determination of the ζ potential by electrophoresis measurements on colloidal solutions of sensitized nanoparticles qualitatively unveiled the electric double layer patterns at the nanoparticle/bulk interface specific to the adorption-capable ionic pairs such as the present dyes. A chromophore coupled to a free, easily solvable anion like **1Me-BF$_4$** quickly desorbed from the surface in an acetonitrile-based concentrated Br_3^-/Br^- DSSC solvent. On the other hand, the hydrophilicity of Br^- and the mild adsorption potential of TfO^- allowed **1Me**$^+$ to desorb at a lower rate, and the strong adsorption potential of TFA^-

afforded the best stabilization for this chromophore. Nonetheless, better results were achieved with the **2Me**$^+$ and **1Dec**$^+$ derivatives, and the substitution by *n*-decyl was found critical for stabilization of the dye at the interface thanks to an enhanced lipophilicity, disrupting its ability to diffuse away in the highly ionic electrolyte. On the other hand, no further experiments were carried out to fully explain the better stabilization of the **2Me**$^+$ derivative. Antagonistically, the stabilization of these derivatives did not improve the DSSC photoaction due a mismatch between energy levels: A necessary driving force for electron injection of ca. 0.2 V between the excited state of the dye and the Fermi level of TiO_2 should be observed for achievement of high IPCEs.[73] We presently aim at designing and characterizing malachite green derivatives with more negative excited state redox levels, more adapted to DSSC use.

Supporting Information

Details of X-ray data collection and reduction for the single crystalline sample of **1Me-Br·Cl$_4$HQ**. Detailed syntheses of all compounds, ^{1}H/^{13}C NMR spectra of the dyes and syntheses intermediates, cyclic voltammetry of the chromophores, FTIR spectroscopy of the dyes in solid state dyes@TiO_2 and syntheses intermediates and raw plotting of the intensity of the zeta potential values and Bode phase plots of the DSSCs.

Acknowledgement

This work was financially supported in part by Grants-in-Aid for Scientific Research (No. 15K05483) from the Ministry of Education, Culture, Sports, Science and Technology of Japan.

References

1 M. J. S. Dewar, *J. Chem. Soc.* **1950**, 2329-2334.

2 D. F. Duxbury, *Chem. Rev.* **1993**, *93*, 381-433.

3 Z.-S. Wang, K. Sayama, H. Sugihara, *J. Phys. Chem. B* **2005**, *109*, 22449-22455.

4 K. R. Mulhern, M. R. Detty, D. F. Watson, *J. Phys. Chem. C* **2011**, *115*, 6010-6018.

5 K. R. Mulhern, A. Orchard, D. F. Watson, M. R. Detty, *Langmuir* **2012**, *28*, 7071-7082.

6 M. W. Kryman, J. N. Nasca, D. F. Watson, M. R. Detty, *Langmuir* **2016**, *32*, 1521-1532.

7 H. Abdulelah, B. Ali, M. A. Mahdi, A. Q. Abdullah, J. J. Hassan, H. F. Al-Taay, P. Jennings, *Journal of Solar Energy* **2016**, *2016*, 7.

8 M. Shimura, K. Shakushiro, Y. Shimura, *J. Appl. Electrochem.* **1986**, *16*, 683-692.

9 P. Ren, Y. Li, Y. Zhang, H. Wang, Q. Wang, *Int. J. Photoenergy* **2016**, *2016*, 2135847.

10 M. S. Roy, P. Balraju, M. Kumar, G. D. Sharma, *Sol. Energy Mater. Sol. Cells* **2008**, *92*, 909-913.

11 G. Ramakrishna, H. N. Ghosh, A. K. Singh, D. K. Palit, J. P. Mittal, *J. Phys. Chem. B* **2001**, *105*, 12786-12796.

12 P. M. Sirimanne, *Renew. Energ.* **2008**, *33*, 1424-1428.

13 P. M. Jayaweera, S. S. Palayangoda, K. Tennakone, *J. Photochem. Photobiol. A* **2001**, *140*, 173-177.

14 S. M. Reda, S. A. El-Sherbieny, *J. Mater. Res.* **2010**, *25*, 522-528.

15 M. Y. El Zayat, A. O. Saed, M. S. El-Dessouki, *Int. J. Hydrogen Energy* **1998**, *23*, 259-266.

16 M. K. Nazeeruddin, R. Humphry-Baker, P. Liska, M. Grätzel, *J. Phys. Chem. B* **2003**, *107*, 8981-8987.

17 M. K. Nazeeruddin, S. M. Zakeeruddin, R. Humphry-Baker, M. Jirousek, P. Liska, N. Vlachopoulos, V. Shklover, C.-H. Fischer, M. Grätzel, *Inorg. Chem.* **1999**, *38*, 6298-6305.

18 *Semiconductor Photochemistry and Photophysics Vol. 10*. V. Ramamurthy, K. S. Schanze, Marcel Dekker, Inc., New York, Basel, **2003**.

19 G. R. Fulmer, A. J. M. Miller, N. H. Sherden, H. E. Gottlieb, A. Nudelman, B. M. Stoltz, J. E. Bercaw, K. I. Goldberg, *Organometallics* **2010**, *29*, 2176-2179.

20 D. B. G. Williams, M. Lawton, *J. Org. Chem.* **2010**, *75*, 8351-8354.

21 D. Zhu, Y. Mu, Q. Li, X. Pang, X. Wang, Y. Liu, G. Chen, H. Chen, *Anal. Methods-UK* **2016**, *8*, 6236-6243.

22 W. Müller, I. Hattesohl, H. J. Schuetz, G. Meyer, *Nucleic Acids Res.* **1981**, *9*, 95-119.

23 J. E. Kuder, W. W. Limburg, M. Stolka, S. R. Turner, *J. Org. Chem.* **1979**, *44*, 761-766.

24 H. Kast, Patent US4000135 A, **1976**.

25 N. M. Cuong, S. Ishizaka, N. Kitamura, *American Journal of Analytical Chemistry* **2012**, *3*, 18256 (7 pages).

26 G. Hallas, K. N. Paskins, D. R. Waring, *J. Chem. Soc., Perkin Trans. 2* **1972**, 2281-2286.

27 S. G. R. Guinot, J. D. Hepworth, M. Wainwright, *J. Chem. Soc., Perkin Trans. 2* **1998**, 297-304.

28 A. G. Kraus, I. Jeon, M. Nilsen-Hamilton, M. A. Awad, J. Banerjee, B. Parvin, *Molecules* **2008**, *13*.

29 L. Yong, G. Zhanqi, J. Yuefei, H. Xiaobin, S. Cheng, Y. Shaogui, W. Lianhong, W. Qingeng, F. Die, *J. Hazard Mater.* **2015**, *285*, 127-136.

30 J.-M. Aubry, B. Mandard-Cazin, M. Rougee, R. V. Bensasson, *J. Am. Chem. Soc.* **1995**, *117*, 9159-9164.

31 G. Schwen, G. Schmidt, *J. Soc. Dyers Colour.* **1959**, *75*, 101-105.

32 M. Yoshizawa, K. Suzuki, A. Kubo, S. Saikan, *Chem. Phys. Lett.* **1998**, *290*, 43-48.

33 G. Li, D. Magana, R. B. Dyer, *J. Phys. Chem. B* **2012**, *116*, 12590-12596.

34 P. Singhal, H. N. Ghosh, *Phys. Chem. Chem. Phys.* **2014**, *16*, 16824-16831.

35 M. Ucak-Astarlioglu, S. Edwards, C. A. Zoto, *Journal of Laboratory Chemical Education* **2017**, *5*, 32–39.

36 B. M. Fox, J. D. Hepworth, D. Mason, J. Sawyer, G. Hallas, *J. Soc. Dyers Colour.* **1982**, *98*, 10-13.

37 E. B. Knott, *J. Chem. Soc.* **1951**, 1024-1028.

38 M. J. Frisch, G. W. Trucks, H. B. Schlegel, G. E. Scuseria, M. A. Robb, J. R. Cheeseman, G. Scalmani, V. Barone, B. Mennucci, G. A. Petersson, H. Nakatsuji, M. Caricato, X. Li, H. P. Hratchian, A. F. Izmaylov, J. Bloino, G.

Zheng, J. L. Sonnenberg, M. Hada, M. Ehara, K. Toyota, R. Fukuda, J. Hasegawa, M. Ishida, T. Nakajima, Y. Honda, O. Kitao, H. Nakai, T. Vreven, J. A. Montgomery, J. E. Peralta, F. Ogliaro, M. Bearpark, J. J. Heyd, E. Brothers, K. N. Kudin, V. N. Staroverov, R. Kobayashi, J. Normand, K. Raghavachari, A. Rendell, J. C. Burant, S. S. Iyengar, J. Tomasi, M. Cossi, N. Rega, J. M. Millam, M. Klene, J. E. Knox, J. B. Cross, V. Bakken, C. Adamo, J. Jaramillo, R. Gomperts, R. E. Stratmann, O. Yazyev, A. J. Austin, R. Cammi, C. Pomelli, J. W. Ochterski, R. L. Martin, K. Morokuma, V. G. Zakrzewski, G. A. Voth, P. Salvador, J. J. Dannenberg, S. Dapprich, A. D. Daniels, Farkas, J. B. Foresman, J. V. Ortiz, J. Cioslowski, D. J. Fox, Gaussian 09, Gaussian, Inc., Wallingford, CT, **2010**.

39 M. K. Nazeeruddin, P. Péchy, T. Renouard, S. M. Zakeeruddin, R. Humphry-Baker, P. Comte, P. Liska, L. Cevey, E. Costa, V. Shklover, L. Spiccia, G. B. Deacon, C. A. Bignozzi, M. Grätzel, *J. Am. Chem. Soc.* **2001**, *123*, 1613-1624.

40 B. O'Regan, M. Gratzel, *Nature* **1991**, *353*, 737-740.

41 J. Lim, Y. S. Kwon, S.-H. Park, I. Y. Song, J. Choi, T. Park, *Langmuir* **2011**, *27*, 14647-14653.

42 A. Hagfeldt, G. Boschloo, L. Sun, L. Kloo, H. Pettersson, *Chem. Rev.* **2010**, *110*, 6595-6663.

43 A. Mishra, M. K. R. Fischer, P. Bäuerle, *Angew. Chem. Int. Ed. Engl.* **2009**, *48*, 2474-2499.

44 N. Heo, Y. Jun, J. H. Park, *Sci. Rep.* **2013**, *3*, 1712.

45 P. M. Sommeling, M. Späth, H. J. P. Smit, N. J. Bakker, J. M. Kroon, *J. Photochem. Photobiol. A* **2004**, *164*, 137-144.

46 J. Lim, Y. S. Kwon, T. Park, *Chem. Commun.* **2011**, *47*, 4147-4149.

47 P. Debye, E. Hückel, *Phys. Z.* **1923**, *24*, 185–206.

48 M. Gouy, *J. Phys. Theor. Appl.* **1910**, *9*, 457-468.

49 D. L. Chapman, *Philos. Mag.* **1913**, *25*, 475-481.

50 D. C. Grahame, *Chem. Rev.* **1947**, *41*, 441-501.

51 L. S. Ornstein, F. Zernike, *Koninklijke Nederlandsche Akademie van Wetenschappen Proceedings* **1914**, *17*, 793–806.

52 G. Trefalt, S. H. Behrens, M. Borkovec, *Langmuir* **2016**, *32*, 380-400.

53 W. Schmickler, R. Guidelli, *J. Electroanal. Chem. Interfacial Electrochem.* **1987**, *235*, 387-392.

54 M. Boström, B. W. Ninham, *Langmuir* **2004**, *20*, 7569-7574.

55 P. Attard, D. Antelmi, I. Larson, *Langmuir* **2000**, *16*, 1542-1552.

56 D. A. H. Hanaor, W. Chrzanowski, Y. Gan, *J. Aust. Ceram. Soc.* **2015**, *51*, 88–93.

57 J.-B. Harlé, S. Mine, T. Kamegawa, V. T. Nguyen, T. Maeda, H. Nakazumi, H. Fujiwara, *J. Phys. Chem. C* **2017**, *121*, 15049-15062.

58 B. J. Hathaway, D. E. Webster, *Proc. Chem. Soc.* **1963**, 14.

59 M. Kosmulski, J. B. Rosenholm, *J. Phys. Chem.* **1996**, *100*, 11681-11687.

60 E. Ronca, M. Pastore, L. Belpassi, F. Tarantelli, F. De Angelis, *Energy Environ. Sci.* **2013**, *6*, 183-193.

61 L. Zhang, J. M. Cole, C. Dai, *ACS Appl. Mater. Interfaces* **2014**, *6*, 7535-7546.

62 M. Pastore, F. De Angelis, *ACS Nano* **2010**, *4*, 556-562.

63 G. B. Deacon, R. J. Phillips, *Coord. Chem. Rev.* **1980**, *33*, 227-250.

64 K. Kakiage, T. Tokutome, S. Iwamoto, T. Kyomen, M. Hanaya, *Chem. Commun.* **2013**, *49*, 179-180.

65 A. Yella, H.-W. Lee, H. N. Tsao, C. Yi, A. K. Chandiran, M. K. Nazeeruddin, E. W.-G. Diau, C.-Y. Yeh, S. M. Zakeeruddin, M. Grätzel, *Science* **2011**, *334*, 629-634.

66 W. Wu, J. Hua, Y. Jin, W. Zhan, H. Tian, *Photochem. Photobio. Sci.* **2008**, *7*, 63-68.

67 X. Ma, J. Hua, W. Wu, Y. Jin, F. Meng, W. Zhan, H. Tian, *Tetrahedron* **2008**, *64*, 345-350.

68 F. S. Meng, Q. H. Yao, J. G. Shen, F. L. Li, C. H. Huang, K. C. Chen, H. Tian, *Synth. Met.* **2003**, *137*, 1543-1544.

69 Y.-S. Chen, C. Li, Z.-H. Zeng, W.-B. Wang, X.-S. Wang, B.-W. Zhang, *J. Mater. Chem.* **2005**, *15*, 1654-1661.

70 Y. Nagasawa, Y. Ando, T. Okada, *Chem. Phys. Lett.* **1999**, *312*, 161-168.

71 M. A. Bell, B. Crystall, G. Rumbles, G. Porter, D. R. Klug, *Chem. Phys. Lett.* **1994**, *221*, 15-22.

72 B.-B. Xie, S.-H. Xia, L.-H. Liu, G. Cui, *J. Phys. Chem. A* **2015**, *119*, 5607-5617.

73 K. Hara, T. Sato, R. Katoh, A. Furube, Y. Ohga, A. Shinpo, S. Suga, K. Sayama, H. Sugihara, H. Arakawa, *J. Phys. Chem. B* **2003**, *107*, 597-606.

74 T. Funaki, H. Kusama, N. Onozawa-Komatsuzaki, K. Kasuga, K. Sayama, H. Sugihara, *Eur. J. Inorg. Chem.* **2014**, *2014*, 1303-1311.

75 H. Wang, B. Wang, J. Yu, Y. Hu, C. Xia, J. Zhang, R. Liu, *Sci. Rep.-UK* **2015**, *5*, 9305 (9 pages).

76 R. Kern, R. Sastrawan, J. Ferber, R. Stangl, J. Luther, *Electrochim. Acta* **2002**, *47*, 4139-4277.

77 A. Zaban, M. Greenshtein, J. Bisquert, *ChemPhysChem.* **2003**, *4*, 859-864.

Graphical Abstract

Malachite Green Derivatives for Dye-sensitized Solar Cells: Optoelectronic Characterizations and Persistence on TiO_2

Jean-Baptiste Harlé,* Shuhei Arata, Shinya Mine, Takashi Kamegawa, Van Tay Nguyen, Takeshi Maeda, Hiroyuki Nakazumi, and Hideki Fujiwara*

Derivatives of malachite green were developed for dye-sensitized solar cell, and conjugated to various coordinative (trifluoroacetate [TFA^-], triflate [TfO^-]) and non-coordinative (tetrafluoroborate [BF_4^-], bromide [Br^-]) counterions. Throughout this study, the bearing of the affinity for the surface/affinity for the bulk of both the chromophores and its counterions was scrutinized and found crucial for the stability and efficiency of the cells.

<Diagram>